In-silico Studies of Ursodeoxycholic Acid From Red Sea Weed Jania Rubens By_aina_et Al

Oluwafemi S. Aina

oluwafemiaina100@gmail.com

University of Lagos, Yaba, Lagos, Nigeria https://orcid.org/0000-0002-2988-6496

Research Article

Keywords: Jania rubens, in-silico, ursodeoxycholic acid, acetylcholinesterase, anti-Alzheimer

Posted Date: June 18th, 2025

DOI: https://doi.org/10.21203/rs.3.rs-6898208/v1

Additional Declarations: The authors declare potential competing interests as follows:

Abstract

Alzheimer's disease, one of the neurodegenerative disorders, is marked by the gradual weakening of nerve cells in the brain or peripheral nervous system, along with abnormal protein aggregation. While there have been significant initiatives towards management of the condition, however there is still a dearth of data on candidate phytochemicals and analogues in the treatment of this condition. Herein we present alkaloids derived from the marine algae *Jania rubens* as inhibitors of human acetylcholinesterase in addressing Alzheimer's disease. Using *in-silico* tools like Protox II and SwissADME, forty isolates were screened for toxicity and ADME properties, while molecular docking simulations was performed using PyRx 0.8 AutoDock Vina Wizard and Discovery Studio 2020. A 50 nanoseconds molecular dynamic (MD) simulation was performed on GROMACS via LINUX environment, and CHARMM 36 force field. Ursodeoxycholic acid (AL20), an isolate from *J. rubens*, exhibited strong inhibitory activity against 4ey6 with a binding energy of -8.5 kcal/mol, surpassing standard anti-Alzheimer drugs Donepezil (-8.3 kcal/mol), Galantamine (-7.7 kcal/mol), and Rivastigmine (-6.4 kcal/mol). However, *in-silico* data revealed AL20 to be 73% hepatotoxic. Thereafter, seven derivatives (AL20A-G) were designed to improve properties for drug likeness. The amide analogue, AL20E showed superior inhibitory activity (-9.0 kcal/mol) and non-toxicity compared to AL20 and the standard drugs. This derivative also demonstrated strong interactions with AChE, forming three hydrogen bonds with amino acid residues Pro290, Ser293, and Leu289. The BOILED-Egg model predicted favorable gastrointestinal absorption and blood-brain barrier penetration for AL20E, indicating its potential as a CNS-active drug. Density Functional Theory (DFT) and Molecular dynamics analyses confirmed the chemical stability of AL20E, making it a promising candidate for anti-Alzheimer drug development. This study highlights AL20E; ((4R)-4-((3S,7S,8R,9S,10S,13R,14S,17R)-3,7-dihydroxy-10,13-dimethylhexadecahydro-1H cyclopenta[a]phenanthren-17-yl)pentanamide)) as a non-toxic, acetylcholinesterase inhibitor with enhanced drug-likeness. This study thereby presents AL20E for consideration as a lead compound in the development of novel Alzheimer’s therapeutics.

1.0 INTRODUCTION

Neurodegenerative diseases, especially Alzheimer’s disease (AD) and Parkinson’s disease (PD), are leading causes of death worldwide and are identified by a progressive loss of specific neuronal cell populations due to abnormal protein aggregation within neurons. Alzheimer's disease is the most common cause of dementia in people over 65 years, affecting 55 million humans and increasing at an alarming rate of 10 million cases per year worldwide [1,2]. Based on the cholinergic hypothesis of the pathogenesis of Alzheimer's disease, the clinical features of dementia observed in this disease are ascribed to decrease levels of acetylcholinesterase, a neurotransmitter involved in memory and learning, in the hippocampus and cortex [3].

It is instructive that FDA-approved drugs, (donepezil, galantamine, memantine and rivastigmine) only temporarily improve symptoms by increasing the number of neurotransmitters in the brain.

Ursodeoxycholic acid (UDCA) was observed to prevent the degradation of IKBo, thus leading to the inhibition of NF-KB-dependent gene expression in microglia. The expression of these genes is associated with inflammation, a significant factor in neurodegenerative diseases like Alzheimer's [4]. Acetylcholinesterase inhibitors are commonly employed to partially alleviate symptoms in mild to moderate Alzheimer's disease. They are also used to manage various other forms of dementia and central nervous system disorders, including Parkinson's disease, Lewy body-related dementia, mild cognitive impairment, Down syndrome, Korsakov disease, and vascular dementia [5].

Researchers are currently actively designing, synthesizing and evaluating new bioactive compounds for Alzheimer's treatment having minimal side effects [6]. For instance, UDCA has been found to reduce neuronal loss in prion-infected cerebellar slice cultures [7]. Additionally, in models of acute bilirubin encephalopathy, UDCA treatment has been demonstrated to prevent apoptosis induced by unconjugated bilirubin in astrocytes and fetal neurons isolated from rats [8]. Alkaloids of marine algae are rare and mostly belong to the indole and phenyl ethylamine groups. Additionally, the biological properties of these alkaloids are still emerging [9–10]. This study seeks to develop alkaloid-based compounds derived from marine algae (red seaweed) *Jania rubens* to address neurodegeneration in Alzheimer's and Parkinson's diseases. The research highlights how to identify compounds that have potential to prevent neuronal loss, reduce inflammation, boost neurotransmitter levels, and minimize side effects, with a specific focus on the role of ursodeoxycholic acid (UDCA).

2.0 MATERIALS AND METHODS

2.1 Isolates from Red Seaweed *Jania rubens*

The method used in the extraction and analysis of the phytochemicals of red seaweed *Jania rubens* employed in this study has been reported by El-Din *et al.* (2016) [11]. The chemical names and structures of the forty (40) isolates investigated herein are listed in Table 1 and Fig. 1 respectively.

2.2 Toxicity Analysis of GCMS Phytochemicals from *Jania rubens*

The target phytochemicals were investigated for toxicity by screening using Protox II web server (https://tox-new.charite de/protox_II/). We imputed the SMILES representation of each phytochemical compound from *Jania rubens* drawn using ChemDraw 14.0 and saved in sdf format in the server. Toxicity information retrieved were; hepatoxicity, carcinogenicity, immunotoxicity, mutagenicity and cytotoxicity.

2.3 Preparation of Enzymes and Docking Study

Protein structures used were initially cleaned by removing all solvent molecules and the co-crystallized ligands prior to docking. Molecular docking calculations for the forty compounds with Alzheimer protein, acetylcholinesterase (PDB ID: 4EY6) were undertaken using PyRx (version 0.8) and DS studio 2020, with

a sphere (15 Å radius) that can accommodate the cavity centered on the binding sites of the protein structure. This approach ensured alignment in their conformations. Standard protonation states of the protein based on neutral pH were used in the docking studies. The isolated structures were built using Chemdraw 14.0. Variable orientations of each ligand were searched and ranked based on their re-rank score. For each docking simulation, the maximum number of iterations for the docking algorithm was set to 9, with a maximum population size of 9 mode runs per ligand. The RMSD threshold for multiple poses was set to 1.00 Å.

Table 1
Structural information of phytochemicals investigated from red seaweed *Jania rubens* [11]

Compd.	Name	Molecular Formula	Molecular Weight (g/mol)
1	2-Imidazolidinone,	$C_3H_6N_2O$	86.0940
2	2-cyclohexylpiperidine	$C_{11}H_{21}N$	167.2960
3	methylene chloride,	CH_2C_{l2}	84.9270
4	6-methyl-4-[(4-methylphenyl) sulfonyl]-5-heptenoic acid,	$C_{15}H_{20}O_4S$	296.3810
5	3-(3-hydroxybutyl)-2,4,4trimethyl-2-cyclohexen-1-one,	$C_{13}H_{22}O_2$	210.3170
6	3-ethyl-5-(2-ethylbutyl)-octadecane,	$C_{26}H_{54}$	366.7180
7	heptadecane,	$C_{17}H_{36}$	240.4750
8	hexadecanal,	$C_{16}H_{32}O$	240.4310
9	tetradecanoic acid,	$C_{14}H_{28}O_2$	228.3760
10	9-hexadecenoic acid,	$C_{16}H_{30}O_2$	254.4140
11	pentadecanoic acid	$C_{15}H_{30}O_2$	242.4030
12	3,7,11,15-tetramethyl-2-hexadecen-1-ol,	$C_{20}H_{40}O$	296.5390
13	6,10,14-trimethyl-2-pentadecanone,	$C_{18}H_{36}O$	268.4850
14	Pentadecanal	$C_{15}H_{30}O$	226.4040
15	3-eicosyne	$C_{20}H_{38}$	278.5240
16	hexadecenoic acid	$C_{16}H_{30}O_2$	254.4140
17	9-oximino-2,7-diethoxyfluorene	$C_{17}H_{17}NO_3$	283.3270
18	hexadecanoic acid methyl ester	$C_{17}H_{34}O_2$	270.4570
19	l-(+)-ascorbic acid 2,6-dihexadecanoate,	$C_{38}H_{68}O_8$	652.9540
20	ursodeoxycholic acid	$C_{24}H_{40}O_4$	392.5800
21	methyl 13-octadecenoate	$C_{19}H_{36}O_2$	296.4950
22	Phytol	$C_{20}H_{40}O$	296.5390

Compd.	Name	Molecular Formula	Molecular Weight (g/mol)
23	trans-13-octadecenoic acid	$C_{18}H_{34}O_2$	282.4680
24	octadecanoic acid	$C_{18}H_{36}O_2$	284.4840
25	Heptasiloxane	$H_{16}O_6Si_7$	308.7170
26	octanoic acid	$C_8H_{16}O_2$	144.2140
27	Octasiloxane	$H_{18}O_7Si_8$	354.8170
28	Squalene	$C_{30}H_{50}$	410.7300
29	9,12,15-octadecatrienoic acid	$C_{18}H_{30}O_2$	278.4360
30	oleic acid	$C_{18}H_{34}O_2$	282.4680
31	17-pentatriacontene	$C_{35}H_{70}$	490.9450
32	propanoic acid	$C_3H_6O_2$	74.0790
33	Rhodopsin	$C_{40}H_{58}O$	554.9030
34	Stigmastanol	$C_{29}H_{52}O$	416.7340
35	withaferin A	$C_{28}H_{38}O_6$	470.6060
36	cholest-5-en-3-one	$C_{27}H_{44}O$	384.6480
37	cyclopropanebutanoic acid	$C_7H_{12}O_2$	128.0837
38	pregn-5-ene-3,20-dione	$C_{21}H_{30}O_2$	314.4690
39	2,4,6-decatrienoic acid	$C_{10}H_{14}O_2$	166.2200
40	Demecolcine	$C_{21}H_{25}NO_5$	371.4330

2.4 Structural Modification of Lead Compound AL20

Compound **AL20** as the lead candidate (Table 4) had the highest binding energy − 8.5 kcal/mol leading it to be selected for derivatization due to unfavourable toxicity profiles. Consequently, seven (7) hypothetical compounds (AL20A – AL20G) were generated using ChemDraw 14.0. The structures were saved in the .sdf format, and their corresponding SMILES notations uploaded onto the Protox II web server as outlined in Section 2.2 above to evaluate their toxicity profiles against necessary compliance with drug-likeness rules [12].

2.5 Drug-likeness and Bioactivity

The seven derivative test compounds (AL20A – AL20G) were investigated using their SMILES representations on admetSAR2 webserver (lmmd.ecust.edu.cn/admetsar2) to predict ADME parameters. Furthermore, bioactivity assessment using molinspiration webserver was carried out to determine their potential as candidates for further drug development. Gastro-intestinal and blood-brain barrier characteristics (BOILED-Egg) of the top three (3) lead compounds obtained from AL20 were also obtained and analysed.

2.6 DFT Studies

The geometry optimization of the lead AL20 and top three derivative compounds AL20B, AL20D and AL20E (Fig. 5) were carried out using Gaussian 09W program [13]. Becke' s three parameter hybrid model (B3) with the Lee, Yang and Parr' s (LYP) correlation functional [14] using the Pople' s standard, split-valence triple-zeta basis set. The format included polarization and diffuse function s 6–311 + + G (d,p) basis set [15] in the density functional theory (DFT) calculations. The investigation of each compound's structural electronic data, chemical reactivity, molecular electrostatic potential map, molecular atomic charges and molecular orbital properties were calculated. The simulated results were viewed using Gaussview 6. 0 version software [16a].

2.7 Molecular Dynamics Simulation by GROMACS

The molecular dynamics (MD) simulations of the lead compounds (AL20, AL20E) and reference drug (Donepezil) were investigated against acetylcholinesterase, having a protein (flexible) – ligand interactions stability and flexibility during binding [16b]. GROMACS via LINUX environment was deployed to simulate the conformations, and the CHARMM 36 force field was used to generate the topological data for the complex. Small molecule topology and coordinate information were obtained from the CGENFF (https://cgenff.com/). The macromolecular system was solvated in an aqueous phase using the SPC216 water model (simple point charge) and neutralized using 0.15 M NaCl solution. A dodecahedron box was used to encapsulate the system, and 5000 iterations of steepest descent strategies were used to minimize energy. The equilibrium of ion molecules around the macromolecule was accomplished at 310 K and 1.0 bar utilizing NPT (constant pressure) and NVT (constant volume) setups. A 50 nanoseconds MD simulation was performed to generate structural trajectories for the analysis. Key parameters assessed include the root-mean-square deviation (RMSD), the root mean-square fluctuation (RMSF), the solvent-accessible surface area (SASA), hydrogen bonds (HBs), and the radius of gyration (Rg).

3.0 RESULTS AND DISCUSSION

3.1 Toxicity Analysis and Binding Energy of GCMS Phytochemicals from *Jania rubens*

Toxicity evaluation is an important step in drug identification and development. Isolates from Red Sea weed investigated using Protox II webserver are presented in Table 2, while summary of their binding

energies is given in Table 4. Out of the forty isolates investigated, seven (AL1, AL4, AL5, AL26, AL32, AL37 and AL39) returned as non-toxic relative to the reference standard drugs (Table 3), whereas isolates AL17, AL20, AL35, AL38 and AL40 (Table 2) flouted one or more toxicity limitations.

Table 2: Toxicity Profiles of Some Isolates of Red Sea Weed *Jania rubens*

Target	Prediction/ Probability			
	AL1	**AL4**	**AL5**	**AL 17**
Hepatotoxicity	Inactive (0.85)	Inactive (0.54)	Inactive (0.61)	Inactive (0.64)
Carcinogenicity	Inactive (0.88)	Inactive (0.75)	Inactive (0.68)	Active (0.56)
Immunotoxicity	Inactive (0.99)	Inactive (0.99)	Inactive (0.99)	Inactive (0.72)
Mutagenicity	Inactive (0.52)	Inactive (0.68)	Inactive (0.61)	Active (0.59)
Cytotoxicity	Inactive (0.80)	Inactive (0.71)	Inactive (0.95)	Inactive (0.74)
	AL 20	**AL26**	**AL32**	**AL 35**
Hepatotoxicity	Active (0.73)	Inactive (0.52)	Inactive (0.69)	Inactive (0.93)
Carcinogenicity	Inactive (0.79)	Inactive (0.63)	Inactive (0.76)	Inactive (0.55)
Immunotoxicity	Inactive (0.78)	Inactive (0.99)	Inactive (0.99)	Active (0.99)
Mutagenicity	Inactive (0.56)	Inactive (100)	Inactive (0.93)	Inactive (0.79)
Cytotoxicity	Inactive (0.76)	Inactive (0.74)	Inactive (0.75)	Active (0.87)
	AL37	**AL 38**	**AL39**	**AL 40**
Hepatotoxicity	Inactive (0.59)	Inactive (0.67)	Inactive (0.59)	Inactive (0.68)
Carcinogenicity	Inactive (0.66)	Active (0.56)	Inactive (0.69)	Inactive (0.59)
Immunotoxicity	Inactive (0.99)	Active (0.96)	Inactive (0.99)	Active (0.99)
Mutagenicity	Inactive (0.72)	Inactive (0.99)	Inactive (0.68)	Inactive (0.87)
Cytotoxicity	Inactive (0.76)	Inactive (0.79)	Inactive (0.75)	Active (0.66)

Interestingly, the isolates AL 20, AL 36, AL 17 and AL 35 demonstrated superior activity based on their binding energy against human acetylcholinesterase (PDB ID: 4EY6) enzyme as anti-Alzheimer drug candidate (Table 4) compared against Donepezil, Galantamine and Rivastigmine (anti-Alzheimer standard drugs). Isolate AL20 (ursodeoxycholic acid) was therefore selected as the target moiety for further investigation through derivatization (Fig. 5).

Table 3: Toxicity Compliance of Some Alzheimer's Standard Drugs

Table 4: Human Acetylcholinesterase (4EY6)- *Jania rubens* Isolate Complex Binding Scores

Target	Prediction/ Probability		
	Donepezil	Galantamine	Rivastigmine
Hepatotoxicity	Inactive (0.98)	Inactive (0.93)	Inactive (0.93)
Carcinogenicity	**Active** (0.50)	Inactive (0.65)	Inactive (0.74)
Immunotoxicity	**Active** (0.95)	**Active** (0.98)	**Active** (0.69)
Mutagenicity	Inactive (0.53)	Inactive (0.76)	Inactive (0.70)
Cytotoxicity	**Active** (0.63)	**Active** (0.50)	Inactive (0.66)

4EY6-Isolate Complex	Binding Energy
4ey6_AL20	**-8.5**
4ey6_AL36	**-8.4**
AL17	**-8.3**
AL35	**-8.3**
4ey6_Donepezil	-8.3
AL28	-8.1
AL38	-8.1
AL40	-8
4ey6_Galantamine	-7.7
AL34	-7.3
AL39	-7.1
AL4	-6.9
4ey6_Rivastigmine	-6.4
AL26	-5.7
AL5	-5.5
AL37	-5.3
AL1	-4
AL32	-3.7

The isolate **AL20** (Ursodeoxycholic acid) exhibited highest inhibitory activity against human acetylcholinesterase protein crystal (4EY6) is presented in Fig. 2 along with other high binding bioactive isolates. The three standard reference drugs considered in this study are shown in Fig. 3.

Next was to investigate the drug-likeness analysis of the high binding energy isolates using SwissAdme webserver (http://www.swissadme.ch/index.php). We observed that five of the isolates (AL17, AL20, AL35, AL38 and AL40) fall within the optimal physicochemical space for bioavailability (Fig. 4). All five isolates exhibited high gastrointestinal absorption capability while AL17, AL38 and AL40 showed blood brain barrier permeability (Table 5). However, isolate AL35 violated one of the Ghose rule suggestive of poor oral bioavailability.

Table 5: Active isolates compliance to drug-likeness rules

Isolate	Lipinski	Ghose	Veber	Egan	Muegge	GI abs	BBB perm
AL17	0	0	0	0	0	High	Yes
AL20	**0**	**0**	**0**	**0**	**0**	High	No
AL35	0	1	0	0	0	High	No
AL38	0	0	0	0	0	High	Yes
AL40	0	0	0	0	0	High	Yes

3.2 Toxicity Probability and Bioavailability of Derivatives of AL20 Isolate

Despite its strong acetylcholinesterase inhibition and favorable drug-likeness, isolate AL20 exhibited high hepatotoxicity (73%), prompting the desire for new derivatives of the moiety. Guided by structure-activity relationship (SAR) principles, seven new derivatives of AL20 (AL20A, AL20B, AL20C, AL20D, AL20E, AL20F, AL20G) were designed to achieve reduction in toxicity properties (Fig. 5).

AL20 was modified for example at the carboxylic functional group, to carry a methyl group (AL20A), ketone (AL20B), aldehyde (Al20G), acid chloride (AL20C), amides (AL20E) and ester (AL20F). Additionally, the butanoic acid side chain was removed, and one of the hydroxyl groups was oxidized to a ketone (AL20D). These modifications were to explore improvement in their biocompatibilities.

Virtual toxicity screening of AL20 derivatives using Protox II webserver showed that AL20B, AL20D and AL20E (Table 6) were non-toxic, unlike AL20C, AL20F and AL20G which showed (57–63% hepatoxicity), while AL20A and AL20G showing immunotoxicity (60–69%). Notably, the non-toxic derivatives of AL20 isolate were more biocompatible than the standard Alzheimer's drugs which displayed varying degrees of toxicity ranging from carcinogenicity, immunogenicity to cytotoxicity (Table 3). Donepezil, Galantamine and Rivastigmine are prescription drugs used in early - to mid-stage Alzheimer's disease. However, their inherent toxicity remains a concern. Interestingly, the bioavailability results (Fig. 6) of the all AL20 derivatives possessed excellent drug-likeness properties better than the three standard drugs. Thus, the non-toxic derivatives were subjected to further analysis.

Table 6: Toxicity compliance of AL20 designed derivatives AL20A-AL20G

Target	Prediction/ Probability			
	AL20	AL20A	AL20B	AL20C
Hepatotoxicity	**Active (0.73)**	Inactive (0.66)	**Active (0.63)**	**Active (0.57)**
Carcinogenicity	Inactive (0.79)	Inactive (0.80)	Inactive (0.72)	Inactive (0.66)
Immunotoxicity	Inactive (0.78)	**Active (0.60)**	Inactive (0.83)	Inactive (0.72)
Mutagenicity	Inactive (0.56)	Inactive (0.87)	Inactive (0.78)	Inactive (0.74)
Cytotoxicity	Inactive (0.76)	Inactive (0.89)	Inactive (0.88)	Inactive (0.77)
	AL20D	AL20E	AL20F	AL20G
Hepatotoxicity	Inactive (0.53)	Inactive (0.67)	**Active** (0.62)	**Active** (0.63)
Carcinogenicity	Inactive (0.78)	Inactive (0.63)	Inactive (0.80)	Inactive (0.72)
Immunotoxicity	Inactive (0.53)	Inactive (0.79)	Inactive (0.53)	**Active** (0.69)
Mutagenicity	Inactive (0.94)	Inactive (0.83)	Inactive (0.63)	Inactive (0.78)
Cytotoxicity	Inactive (0.81)	Inactive (0.74)	Inactive (0.67)	Inactive (0.88)

3.3 Bioactivity Score of Derivative Lead Compounds

The bioactivity scores of the lead candidates AL20B, AL20D, AL20E, the isolate AL20 and the reference drug Donepezil are presented in Fig. 7. The evaluation included parameters such as G-protein-coupled receptors (GPCR (**1**)) ligand, ion channel modulator (ICM (**2**)), kinase inhibitor (KI (**3**)), nuclear receptor ligand (NRL (**4**)), protease inhibitor (PI (**5**)) and enzyme inhibitor EI (**6**)). Compounds with bioactivity scores higher than 0.00 is defined as active, those between − 0.50 to 0.0 is moderately active and scores lower than − 0.50 is considered inactive. The lead compounds AL20B, AL20D and AL20E were found to display bioactivity scores that range between − 0.4 -1.0 suggestive of moderate to strong activity. They showed notable activity such as ion-channel modulator (0.2–0.4), protease inhibitor (0.1–0.4), enzyme inhibitor (0.6–0.8) and nuclear receptor ligand (0.6–1.0) relative to donepezil. Additionally, they compete effectively with donepezil as GCPR ligands, derivatives AL20B and AL20D were inactive as kinase inhibitors (KI) (-0.6–0.8).

3.4 BOILED-egg Model for Blood-Brain Barrier Permeability and Gastrointestinal Absorption

The BOILED-Egg method predicts the human gastrointestinal absorption (GI) and blood–brain barrier (BBB) penetration by using the SMILE string of the study compounds. The algorithm uses two physicochemical parameters: lipophilicity (WLOGP) and polarity (TPSA), while It estimates physicochemical descriptors such as brain access and gastrointestinal absorption for compounds; AL20, AL20B, AL20D and AL20E (Fig. 5). The analysis identifies substrate or non-substrate permeability glycoproteins (PGP) which are detected as positive or negative in the brain, or intestine (BOILED-Egg) [17–18]. The statistical robustness, graphical nature and speed of this method permits efficient molecular design translation in drug discovery and medicinal chemistry [17]. Drug-likeness parameters

such as iLOGP, GB/SA, XLOGP3, WLOGP, MLOGP and SILICOS-IT, as well as drug-likeness rules such as; Lipinski, Veber, Muegge, Ghost and Egan are incorporated in the BOILED-EGG tool. The SwissADME tool facilitates pharmacokinetics predictions especially ADME, bioavailability and medicinal chemistry insights [18–19].

More than 98% of small molecules are unable to cross the blood-brain barrier (BBB) [20], making the BBB an essential factor in the drug design process particularly for CNS disorders. The quantity of drug candidates absorbed by the intestinal system is a significant factor for oral bioavailability [21], thereby underlining the import of the GI absorption of the molecules. P-Glycoprotein (PGP) is a member of the ATP Binding Cassette family (ABC) and an ABC transporter [22]. It acts as a biological barrier, pumping out the many toxins and xenobiotics from cells while also contributing to the absorption and extraction of the drugs [23]. The overexpression of ABC transporters causes multidrug resistance (MDR) and is linked to the failure of disease treatments such as cancer [24].

The yellow region in Fig. 8 represents zone of compound having good permeation and absorption ability in both BBB and GI. However, the white region defines good GI absorption but not BBB penetration. Molecules 1 and 4, marked with blue (+) dots, and molecules 2 (AL20) and 3 (AL20D), marked with red (−) dots, indicate that the former are predicted to be effluxed from the Central Nervous System (CNS) by PGP, while the latter are predicted not to be effluxed.

The point to note is that compounds that are expectedly effluxible from CNS all have good permeation and absorption ability. Similarly, compounds depicted in red dots; (AL20 (2) and AL20D (3)), although have good permeation and absorption ability in BBB, were both negatively impacted by PGP.

3.5 Density Functional Theory Measurements of Target Compounds

The molecular geometry optimization for the isolate AL20 derivatives (AL20B, AL20D, and AL20E) were carried out at DFT/B3LYP level of theory with 6–311 + G (d, p) basis set. The optimized molecular geometry of the AL20s is shown in Fig. 9.

The chemical characteristics of the designed compounds AL20B, AL20D and AL20E were analysed using the highest occupied molecular orbital (HOMO) and lowest unoccupied molecular orbital (LUMO) energy levels [25]. This provides insights on the atomic orbital and electron density around the atomic surfaces to define the chemical stability in molecules based on the conceptual-DFT indices [26], such as hardness (η), softness (S), electrophilicity index (ω) and chemical potential (μ).

The global chemical hardness and softness measure the resistance and susceptibility of a molecule to exchange electrons with the other molecules respectively (i.e., they have an inverse relation $S = 1/\eta$) [27]. The electrophilicity index indicates the overall electrophilicity and nucleophilicity of a molecule. Also, the feasibility of intermolecular electron transfer in the ground state is defined by the chemical potential [28]. The chemical reactivity descriptors were summarized in Table 7.

Table 7
The Chemical Reactivity Parameters

Ligands	E_{HOMO}	E_{LUMO}	Δ*E*	IE	EA	H	S	ω	M
AL20B	-0.251	-0.026	0.225	0.251	0.026	0.1125	8.889	0.085	-0.139
AL20D	-0.248	-0.03	0.218	0.248	0.03	0.109	9.174	0.089	-0.139
AL20E	-0.256	-0.015	0.241	0.256	0.015	0.1205	8.299	0.076	-0.136

The band gaps of the designed compounds are small in the increasing order of AL20D < AL20B < AL20E. As shown by the frontier HOMO and LUMO molecular orbitals distribution (Fig. 10), the carbonyl substituents likely enhanced the electrophilicity leading to a lower Δ*E* as indicated in the smaller band gaps in AL20B and AL20D while the larger band gap in AL20E can be explained by the amide substituent which has a smaller electron withdrawing effect compared to carbonyl. Compound AL20E has the highest chemical potential (0.241 eV) (Fig. 10c). The nucleophilicity trend is in the order of AL20D < AL20B < AL20E. The index value of 0.076 for AL20E demonstrates a stronger nucleophilic character compared to AL20B and AL20D. It utilizes this nature for conventional hydrogen bonds with Ser293, Leu289 and Pro290 in interaction with the target receptor. Overall, it can be concluded that the designed compounds have potentials as target drug candidates for Alzheimer disease.

The molecular electrostatic potential (MEP) map provides information on molecular interactions and chemical behavior of molecules with other molecular species [29]. The color gradient ranges from red (high electron density, negative electrostatic potential) to blue (low electron density, positive electrostatic potential), with green representing neutral regions. The MEP map for the AL20 derivatives was computed using DFT/ B3LYP level of theory with 6–311 + + G (d, p) basis set (Fig. 10a-c) The red regions indicate sites for electrophilic attack while the blue regions highlight areas susceptible to nucleophilic interactions. Consistent with the DFT-concept reactivity indices, the blue regions, such as the amino group in AL20E, align with nucleophilic interactions, supporting conventional hydrogen bonds with Ser293, Leu289 and Pro290. Summarily, the maps revealed surfaces of possible interactions of drugs with proteins.

The transition of electrons from HOMO to LUMO energy levels are represented by the electronic distribution on the HOMO and LUMO surfaces (Fig. 10a-c). It is inferred from the surfaces that the lower energy gaps for AL20D and AL20B may be well indicated by the localization of the electron density on the carbonyl or the aliphatic moiety both in the HOMO and LUMO after the transition. That is, the transition is occurring within the same regions or very close regions on the molecular surface. In AL20E, the transition between HOMO to LUMO will result in the transfer of the electron distribution from the carbonyl or aliphatic region to the alicyclic region of the compound. This might explain the higher energy gap in the HOMO-LUMO transition.

3.6 Binding Potentials of Derivatives of Lead Isolate AL20

It was necessary to dock these derivatives expecting if any of those non-toxic derivatives would also provide excellent binding and it was wonderful to note that derivative AL20E performed better than phytochemical AL20 and all the reference drugs (shown in Table 8) as a potential inhibitor of human acetylcholinesterase (4ey6), a significant target for therapeutic drugs.

Table 8: Summary of Docking Results for AL20 hypothetical derivatives

Ligand	Binding Affinity	rmsd/ub	rmsd/lb
4ey6_AL20E	-9	0	0
4ey6_AL20	-8.5	0	0
4ey6_Donepezil	-8.3	0	0
4ey6_AL20B	-8.2	0	0
4ey6_AL20D	-8.1	0	0
4ey6_AL20C	-7.8	0	0
4ey6_AL20A	-7.8	0	0
4ey6_Galantamine	-7.7	0	0
4ey6_AL20F	-7.6	0	0
4ey6_AL20G	-7.3	0	0
4ey6_Rivastigmine	-6.4	0	0

Figure 11 shows the 2D and 3D structures of 4ey6_AL20 complex revealing the lone bonding residue $Tryptophan_{286}$, its bond length, distance and the hydrophobic/ hydrophilic/ solvent surface interactions. The lone interaction is a testament to its lower binding energy when compared with the amide derivative A20E.

It is worth to note that derivative AL20E showed higher binding while also possessing more interacting residues with three strong hydrogen bonds (with $Serine_{293}$, $Leucine_{289}$ and $Proline_{290}$). The non-toxicity and strong interaction of AL20E makes it stand out as potential anti-Alzheimer agent when it passes clinical trials. Figure 12 illustrates the 3D structures of 4ey6_AL20E complex revealing all the key residues ($Tryptophan_{286}$, $Tyrosine_{341}$, $Serine_{293}$, $Leucine_{289}$ and $Proline_{290}$) along with bond length, distance and the hydrophobic/ hydrophilic/ solvent surface interactions.

The 3D binding interactions of derivative AL20E (Fig. 12), which forms strong interactions through π-alkyl and hydrogen bonds with amino acid residues Trp_{286}, Leu_{289}, Pro_{290}, Ser_{293} and Tyr_{341}. The presence of three strong hydrogen bonds is likely to contribute to its highest binding energy. The reference Alzhiemer drugs (Fig. 13) on the other hand interacted through multiple bonds, including π-alkyl, π- π stacked, C-H and hydrogen bonds, but exhibit lower binding energy which could be due to its lone hydrogen bonding and the unfavorable acceptor-acceptor with Tyr_{124}.

Acetylcholine is a neurotransmitter essential for processing memory and learning, is decreased in both concentration and function in patients with Alzheimer's disease. The reduction could contribute to reduction impact of Alzheimer disease [30–31]. The strong hydrogen bonding interaction exhibited by

AL20E is promising in the search for new drug candidates. l-Proline is a known neuromodulator in the brain and fulfills many of the criteria of a classic neurotransmitter [32–33]. The body uses proline to make proteins, such as collagen involved in the general function of the cells [34].

Leucine promotes muscle growth, bone healing, and may help control blood sugar [35]. Additionally, some reports adduce to branched-chain amino acids like leucine may be able to extend lifespan by preventing catabolism [36]. L-Serine supports protein synthesis, neurotransmission, and the synthesis of important molecules [37], and its supplementation has been shown to extend lifespan in C. elegans by stimulating one-carbon metabolism [38].

3.7 Molecular Dynamics of lead compounds and reference drug

Molecular dynamics simulations offer insights into the dynamic behavior of protein-ligand complexes, including structural stability, interaction strength, and thermodynamic properties [39]. In this study, we compare three complexes: 4ey6_AL20 **(black**), 4ey6_AL20E (**red**), and 4ey6_Donepezil (**green**). Donepezil serves as a reference ligand due to its established efficacy as an acetylcholinesterase inhibitor, while AL20 and AL20E represent potential alternatives or improvements. This experiment produced figures for the RMSD, RMSF, hydrogen bonds, SASA and Rg values of protein-ligand complexes. Also, the temperature, pressure and density figures of the system throughout the simulation were also provided.

3.7.1 Stability Analysis: Backbone and Ligand RMSD

The RMSD values of 4ey6_AL20, 4ey6_AL20E and 4ey6_Donepezil for the main (backbone) of 4ey6 (acetylcholinesterase) were fluctuating approximately between 0.12 to 0.24 nm, 0.10 to 0.18 nm and 0.12 to 0.23 nm, with average RMSD values of 0.18nm, 0.14 nm and 0.175 nm. This indicated that the compound, AL20E, having the lowest RSMD value of 0.14 nm, is more stable across the 50 ns simulations compared to AL20 and Donepezil (Fig. 14a).

Similarly, the RMSD values of the ligands AL20, AL20E and Donepezil were predicted, with AL20 starting approximately from 0.4 nm and fluctuated between 0.6 to 1.0 nm, AL20E started at approximately 0.00 nm and slightly fluctuated between 0.5 to 0.8 nm and Donepezil started at approximately 0.2 nm but spiked drastically after 5 ns, showing multiples peaks at 6.0 to 7.5 nm and stabilized slightly around 1.5 to 2.5 nm after 22 ns (Fig. 14b). Therefore, the average RMSD values of AL20, AL20E and Donepezil are 0.7 nm, 0.4 nm and 3.85 nm. Hence, AL20E is the strongest with the most stable interactions as shown in Fig. 14b.

3.7.2 Flexibility: Root mean square fluctuation (RMSF) and Hydrogen Bonding

The RMSF plot shows the flexibility of each residue over a 50 ns simulation (Fig. 15a). 4ey6_AL20 fluctuated mostly below 0.5 nm for most residues, with a peak at residue 80 (0.5 nm) suggesting some

flexibility. 4ey6_AL20E peaks are minimal, and most residues stay below 0.4 nm, but show a peak near residue 400 (0.5 nm), suggesting some flexibility. 4ey6_Donepezil has more fluctuations than 4ey6_AL20 and 4ey6_AL20E, with a small peak near residue 400 (0.5 nm) and a large peak at the C-terminal (2.9 nm). However, the high fluctuation at the ends of 4ey6_Donepezil suggests flexibility or unfolding, making it the least stable but 4ey6_AL20E had the least fluctuation, hence more stable, as shown in Fig. 15a.

Hydrogen bonding analysis for 4ey6_AL20 shows fewer fluctuation, mostly between 1 and 2 hydrogen bonds (Fig. 15b), and there is presence of 3 bonds that fluctuate from 15–18 ns, but slightly fewer than 4ey6_AL20E and 4ey6_Donepezil. 4ey6_AL20E fluctuates between 1 and 3 H-bonds and it peaks at 4 bonds around 20 ns, indicating strong binding interactions. 4ey6_Donepezil has the least fluctuation in hydrogen bonds, noticeable between 1 and 2 hydrogen bonds, and a single 3 hydrogen bonds at 2 ns. Therefore, in this hydrogen bond analysis, 4ey6_AL20E exhibits the highest and most consistent hydrogen bond count, consistent with capacity for strong binding strength, as shown in Fig. 15b.

3.7.3 Compactness: Radius of Gyration (Rg) and Solvent Accessibility (SASA).

Rg value (Fig. 16a) for 4ey6_AL20 ranges between 2.30–2.32 nm with minimal fluctuations; that of 4ey6_AL20E maintains a consistent Rg value around 2.30–2.32 nm with very few deviations and 4ey6_Donepezil starts around 2.30 nm and exhibits significant fluctuations between 2.30–2.37 nm around the 10,000–20,000 ps (10–20 ns) but stabilizes towards the end of the simulation. 4ey6_AL20E displays similar Rg values to 4ey6_AL20 but with slightly reduced fluctuations, reflecting improved structural integrity. Therefore, 4ey6_AL20E is more compact and stable than 4ey6_AL20 and 4ey6_Donepezil as shown in Fig. 16a.

Also, SASA indicates how much of the protein's surface is exposed to solvent, and as shown in Fig. 16b; 4ey6_AL20 had SASA value that fluctuates between 215 to 230 nm², 4ey6_AL20E value which ranges from 210 to 225 nm² and 4ey6_Donepezil increases from 202 nm² to 234 nm² for the first 20ns and became stable for the rest for the simulation. The SASA values for 4ey6_AL20 and 4ey6_AL20E are high but they’re less exposed to solvent compared to 4ey6_Donepezil (Fig. 16b).

3.7.4 Thermodynamic Stability/ Energy Profiles

The Gromacs energies, starting from the temperature (Fig. 17a) of 4ey6_AL20, 4ey6_AL20E and Donepezil, presented a stable temperature, with minimal fluctuations around 300 K throughout the 50,000 ps (50 ns) simulation, indicating proper temperature coupling and stable thermal conditions. The pressure plot (Fig. 17b) shows significant fluctuations between − 400 bar and 400 bar for 4ey6_AL20, 4ey6_AL20E and Donepezil. The density plot for 4ey6_AL20, 4ey6_AL20E and Donepezil, remains stable around 1044 kg/m³ as shown in Fig. 17c. This indicated that the system was stable throughout the 50,000 ps (50 ns) simulations but some slight increase in pressure was noticed.

From the comparison of molecular dynamics results, AL20E exhibits highest stability, reduced flexibility, higher hydrogen bond counts, compactness and optimal energy levels, reaffirming its effectiveness as acetylcholinesterase inhibitor.

Conclusion

In this work we examined the potential of alkaloids identified from marine algae (red seaweed *Jania rubens*) as inhibitors of human acetylcholinesterase, a target in neurodegenerative diseases. GCMS reported isolates were evaluated for toxicity and ADME properties using *in-silico* tools. DFT studies, molecular docking and molecular dynamics simulations were performed to identify potential new phytochemical compounds and analogues as candidates for therapeutic intervention of neurodegenerative diseases like Alzheimer's. Seven analogues of UDCA (AL20A-AL20G) were designed to improve the isolates drug-likeness. Further *in-silico* investigation revealed the keto (AL20B), amide (AL20E) and the cleaved analogue (AL20D) to have better toxicity profiles. Donepezil an FDA approved reference compound exhibited only one hydrogen bonding with Arg_{296} in hydrophobic interaction at a lower solvent accessibility surface. However, AL20E indicated three strong hydrogen bonds with amino acid residues Pro_{290}, Ser_{293}, Leu_{289} located within the hydrophobic region and higher solvent accessibility surface of the human acetylcholinesterase protein. The hydrogen bonding from the MD study showed good stability for AL20E. The BOILED-Egg model revealed compounds AL20 (1) and AL20E (4) will significantly be effluxed from GI while also possessing good GI absorption and permeation ability with positive impact by PGP. Finally, AL20E; **((4R)-4-((3S,7S,8R,9S,10S,13R,14S,17R)-3,7-dihydroxy-10,13-dimethylhexadecahydro-1H-cyclopenta [a]phenanthren-17-yl)pentanamide)** investigated in this *in silico* study outperformed Donepezil (including the other two FDA approved Alzhiemer's drugs) and AL20 by possessing far better binding energy and drug-likeness characteristics is therefore recommended for further exploratory studies as a potential anti-alzheimer drug candidate.

Declarations

Acknowledgements

The authors wish to appreciate the Royal Society of Chemistry, Computer Laboratory at the D. K. Olukoya Central Research & Reference Laboratories, University of Lagos for supporting this research.

The authors declare that this article represents their own work and does not reflect the policies or views of any individual or organization

Competing Interest

The authors of the article stated that there is no competing interest.

Funding

No was received for this manuscript preparation.

Authors' Contribution statements

The virtual screening studies (toxicity and docking studies) of the compounds was carried out by OSA carried whilst OWE, LAA and OBF conceptualized the studies. LAA and OBF supervised the studies. LAA provided instrumentation for experimental studies, MOR generated the DFT data and interpreted it, NOB generated the dynamics data while OSA interpreted it. OSA and OWE wrote the first manuscript draft. OSA, KO-F, OAI, NOB and LAA critically reviewed and edited the manuscript.

References

1. Li, B., He, D. J., Li, X. J., and Guo, X. Y. (2022). Modeling neurodegenerative diseases using non-human primates: advances and challenges. Ageing and Neurodegenerative Diseases, 2022, 2 (3), 12.
2. Kumar, Astik, et al. "Current and future nano-carrier-based approaches in the treatment of Alzheimer's disease." Brain Sciences, 2023, 13(2)213.
3. Martorana, A., Esposito, Z., and Koch, G. Beyond the cholinergic hypothesis: do current drugs work in Alzheimer's disease?. CNS neuroscience & therapeutics, 2010, *16* (4), 235-245.
4. Joo, S. S., Won, T. J., and Lee, D. I. Potential role of ursodeoxycholic acid in suppression of nuclear factor kappa B in microglial cell line (BV-2). Archives of pharmacal research, 2004, 27, 954-960.
5. Giacobini, E. Cholinesterase inhibitors: new roles and therapeutic alternatives. Pharmacological research, 2004, 50 (4), 433-440.
6. Bores, G. M., Huger, F. P., Petko, W., Mutlib, A. E., Camacho, F., Rush, D. K., ... and Vargas, H. M.. Pharmacological evaluation of novel Alzheimer's disease therapeutics: acetylcholinesterase inhibitors related to galanthamine. Journal of Pharmacology and Experimental Therapeutics, 1996, 277 (2), 728-738.
7. Cortez, L. M., Campeau, J., Norman, G., Kalayil, M., Van der Merwe, J., McKenzie, D., and Sim, V. L. Bile acids reduce prion conversion, reduce neuronal loss, and prolong male survival in models of prion disease. Journal of virology, 2015, 89 (15), 7660-7672.
8. Silva, R. F., Rodrigues, C. M., and Brites, D. Bilirubin-induced apoptosis in cultured rat neural cells is aggravated by chenodeoxycholic acid but prevented by ursodeoxycholic acid. Journal of hepatology, 2001, 34 (3), 402-408.
9. Guven, K. C., Percot, A., and Sezik, E. Alkaloids in marine algae. Marine Drugs, 2010, 8 (2), 269-284.
10. Souza, C. R., Bezerra, W. P., and Souto, J. T. Marine alkaloids with anti-inflammatory activity: Current knowledge and future perspectives. Marine Drugs, 2020, 18 (3), 147.
11. El-Din, S. M. M., and El-Ahwany, A. M. Bioactivity and phytochemical constituents of marine red seaweeds (Jania rubens, Corallina mediterranea and Pterocladia capillacea). Journal of Taibah University for Science, 2016, 10(4), 471-484.

12. Lipinski B, Herzog H, Kops ER, et al., Expectation maximization reconstruction of positron emission tomography images using anatomical magnetic resonance information. IEEE Trans Med Imaging, 1997, 16: 129–136.
13. Frisch, M. J. Trucks,G.W., H. B. Schlegel, G. E. Scuseria, M. A. Robb, J. R. Cheeseman, G. Scalmani, V. Barone, B. Mennucci, G. A. Petersson, H. Nakatsuji, M. Caricato, X. Li, H. P. Hratchian, A. F. Izmaylov, J. Bloino, G. Zheng, J. L. Sonnenberg, M. Hada, M. Ehara, K. Toyota, R. Fukuda, J. Hasegawa, M. Ishida, T. Nakajima, Y. Honda, O. Kitao, H. Nakai, T. Vreven, J. A. Montgomery Jr., J. E. Peralta, F. Ogliaro, M. Bearpark, J. J. Heyd, E. Brothers, K. N. Kudin, V. N. Staroverov, R. Kobayashi, J. Normand, K. Raghavachari, A. Rendell, J. C. Burant, S. S. Iyengar, J. Tomasi, M. Cossi, N. Rega, J. M. Millam, M. Klene,J. E. Knox, J. B. Cross, V. Bakken, C. Adamo, J. Jaramil, R. Gomperts, R. E. Stratmann, O. Yazyev, A. J. Austin, R. Cammi, C. Pomelli, J. W. Ochterski, R. L. Martin, K. Morokuma, V. G. Zakrzewski, G. A. Voth, P. Salvador, J. J. Dannenberg, S. Dapprich, A. D. Daniels, O. Farkas, J. B. Foresman, J. V. Ortiz, J. Cioslowski, and D. J. Fox, (2010) Gaussian 09, Revision B.01. Gaussian Inc., Wallingford.
14. Rivero, P., Moreira, I. D. P., Illas, F., and Scuseria, G. E. Reliability of range-separated hybrid functionals for describing magnetic coupling in molecular systems. The Journal of chemical physics, 2008, 129 (18).
15. Bielecki, J., and Lipiec, E.. Basis set dependence using DFT/B3LYP calculations to model the Raman spectrum of thymine. Journal of Bioinformatics and Computational Biology, 2016, 14 (01), 1650002.
16. a García-Valverde, M., Cordero, N. A., and de la Cal, E. S.. GAUSSVIEW® as a tool for learning organic chemistry. In *EDULEARN15 Proceedings,* 2015, 4366-4370.b Bekker, H, Berendsen, H. J. C., Dijkstra, E. J., Achterop, S., Vondrumen, R. V., Vanderspoel, D., Renardus, M. K. R. (1993). Gromacs-a parallel computer for molecular-dynamics simulations. Proceedings of the 4th International Conference on Computational Physics (PC 92), 252-256.
17. Daina, A., & Zoete, V. A boiled-egg to predict gastrointestinal absorption and brain penetration of small molecules. ChemMedChem, 2016, 11(11), 1117-1121.
18. Daina, A., Michielin, O. and Zoete, V. “iLOGP: A simple, robust, and efficient description of n-octanol/water partition coefficient for drug design using the GB/SA approach”, Journal of Chemical Information and Modelling 2014, 22 (54), 3284-330.
19. Lipinski, C.A., Lombardo, F., Dominy, B.W., and Feeney, P.J. (2001). “Experimental and computational approaches to estimate solubility and permeability in drug discovery and development settings”, Advanced Drug Delivery Reviews, 2001, 1 (46) 326.
20. Pardridge, W.M. The blood-brain barrier: bottleneck in brain drug development, NeuroRx, 2015, 2 (1) 3–14.
21. Barthe, L., Woodley, J. and Houin, G. Gastrointestinal absorption of drugs: methods and studies. Fundam. Clin. Pharmacol. 1999, 13 (2), 154–168.
22. Mollazadeh, S., Sahebkar, A., Hadizadeh, F., Behravan, J. and Arabzadeh S. Structural and functional aspects of P-glycoprotein and its inhibitors, Life Sci. 2018, 214, 118–123.

23. Lin, J. H. and Yamazaki, M. Role of P-glycoprotein in pharmacokinetics: clinical implications, Clin. Pharmacokinet, 2003, 42 (1), 59–98.
24. Dong, J., Qin, Z., Zhang, W. D., Cheng, G., Yehuda, A.G., Ashby, C.R., Chen, Z. S., Cheng, X. D. and Qin, J. J. Medicinal chemistry strategies to discover P-glycoprotein inhibitors: an update, Drug Resist. Updates, 2020, 49, 100681.
25. Aina, O. S., Rofiu, M. O., Oloba-Whenu, O. A., Olasupo, I. A., Adams, L. A., & Familoni, O. B. Drug design and in-silico study of 2-alkoxylatedquinoline-3-carbaldehyde compounds: Inhibitors of Mycobacterium tuberculosis. Scientific African 2024, 23, E01985.
26. Geerlings, P., Chamorro, E., Chattaraj, P. K., De Proft, F., Gázquez, J. L., Liu, S., ... and Ayers, P. Conceptual density functional theory: status, prospects, issues. Theoretical Chemistry Accounts, 2020, 139 (2), 36.
27. Pal, R., and Chattaraj, P. K. Electrophilicity index revisited. Journal of Computational Chemistry, 2023, 44 (3), 278-297.
28. Galabov, B., Ilieva, S., Koleva, G., Allen, W. D., Schaefer III, H. F., and Von R. Schleyer, P. Structure–reactivity relationships for aromatic molecules: electrostatic potentials at nuclei and electrophile affinity indices. Wiley Interdisciplinary Reviews: Computational Molecular Science, 2013, 3(1), 37-55.
29. Dos Santos, M. A. B., de Oliveira, L. F. S., de Figueiredo, A. F., dos Santos Gil, F., de Souza Farias, M., Bitencourt, H. R., ... and Ciríaco-Pinheiro, J. Molecular electrostatic potential and chemometric techniques as tools to design bioactive compounds. In Cheminformatics and its Applications. IntechOpen, 2019.
30. Francis PT. The interplay of neurotransmitters in Alzheimer's disease. CNS Spectr. 2005, 10 (11) 6-9. doi: 10.1017/s1092852900014164.
31. Stanciu GD, Luca A, Rusu RN, Bild V, Beschea Chiriac SI, Solcan C, Bild W, Ababei DC. Alzheimer's Disease Pharmacotherapy in Relation to Cholinergic System Involvement. Biomolecules. 2019, 10(1):40. doi: 10.3390/biom10010040.
32. Johnson J.L. and Roberts E. Proline, glutamate and glutamine metabolism in mouse brain synaptosomes. Brain Res. 1984;323:247–256. doi: 10.1016/0006-8993(84)90295-6.
33. Takemoto Y., Semba R. Immunohistochemical evidence for the localization of neurons containing the putative transmitter L-proline in rat brain. *Brain Res.* 2006;1073:311–315. doi: 10.1016/j.brainres.2005.12.064.
34. Albaugh VL, Mukherjee K and Barbul A. Proline precursors and collagen synthesis: Biochemical challenges of nutrient supplementation and wound healing. J Nutr. 2017;147(11):2011-2017. Doi: 10.3945/jn.117.256404.
35. Duan Y, Li F, Li Y, Tang Y, Kong X, Feng Z, Anthony TG, Watford M, Hou Y, Wu G, Yin Y. The role of leucine and its metabolites in protein and energy metabolism. Amino Acids. 2016, 48(1):41-51. doi: 10.1007/s00726-015-2067-1.
36. Mansfeld, J.Urban, N. Priebe, S. Groth, M. Frahm, C. Hartmann, N. Gebauer, J. Ravichandran, M.Dommaschk, A. Schmeisser, S. Kuhlow, D. Monajembashi, S. Bremer-Streck, S.Hemmerich, P.

37. Holeček M. Serine Metabolism in Health and Disease and as a Conditionally Essential Amino Acid. Nutrients, 2022, 14(9):1987. doi: 10.3390/nu14091987.
38. Liu, Y.L.Janssens, G.E. McIntyre, R.L. Molenaars, M. Kamble, R. Gao, A. W. Jongejan, A. Weeghel, M. V. MacInnes, A. W. and Houtkooper R. H. Glycine promotes longevity in Caenorhabditis elegans in a methionine cycle-dependent fashion. PLoS Genet., 2019, 15 (3), e100763.
39. Berendsen, H. J., van der Spoel, D. and van Drunen, R. (1995). GROMACS: a message-passing parallel molecular dynamics implementation Comput. Phys. Commun., 91 (1–3), 43-56.

Figures

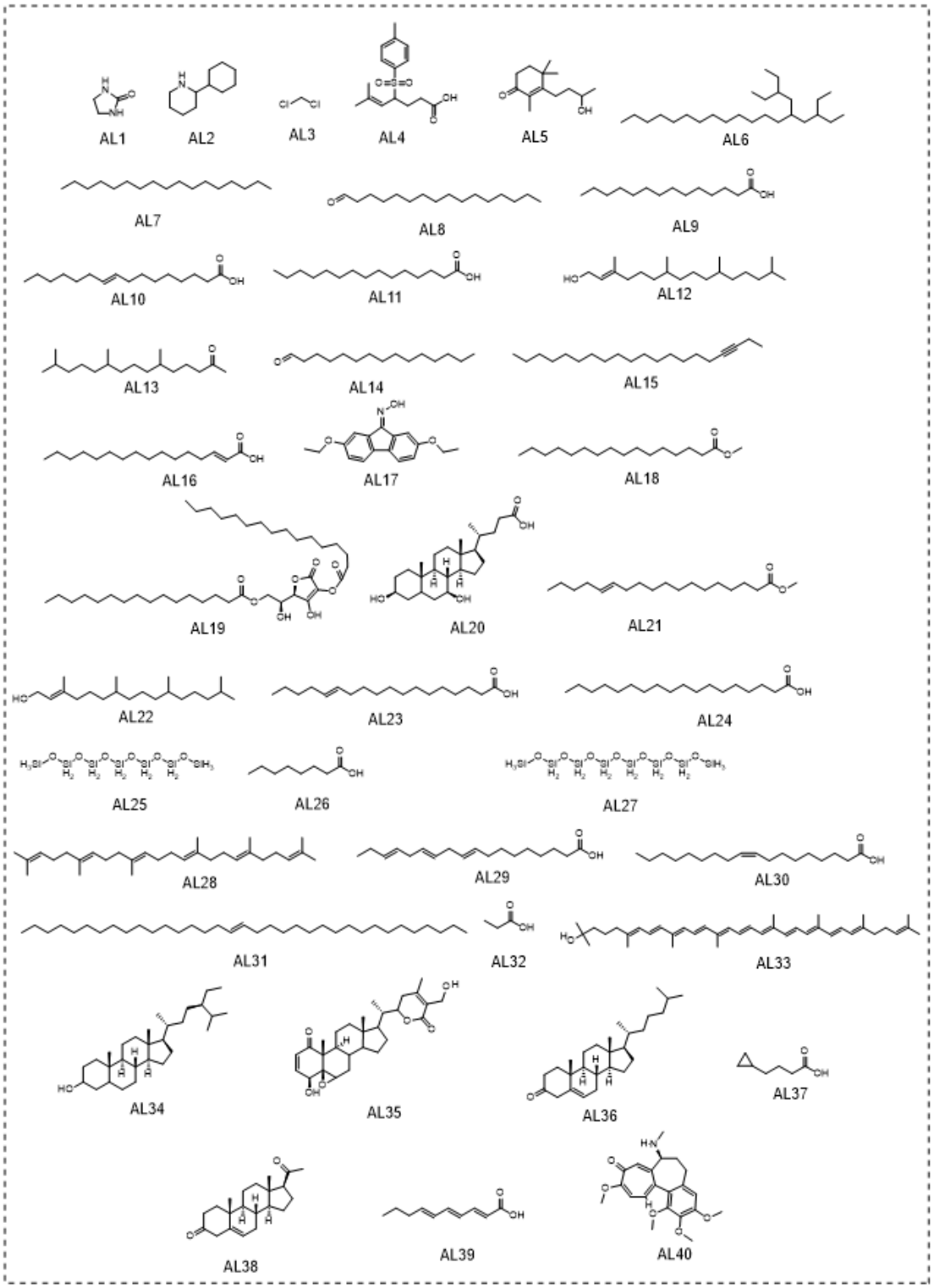

Figure 1

Molecular structures of isolated compounds obtained from Red Seaweed *Jania rubens*

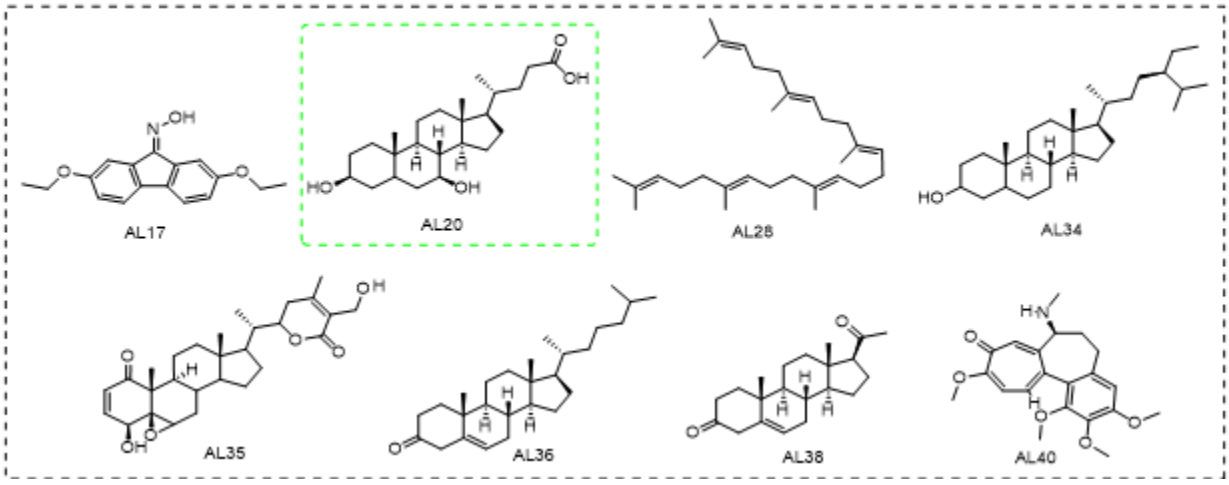

Figure 2

Bioactive isolates of *Jania rubens* against human acetylcholinesterase

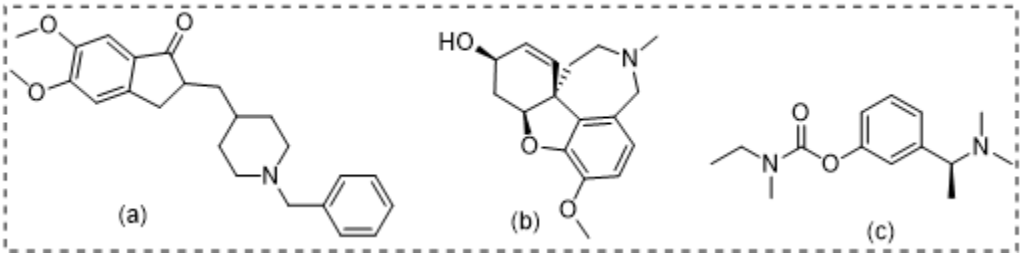

Figure 3

Structures of commonly used Alzheimer's drugs, (a) Donepezil, (b) Galantamine, and (c) Rivastigmine.

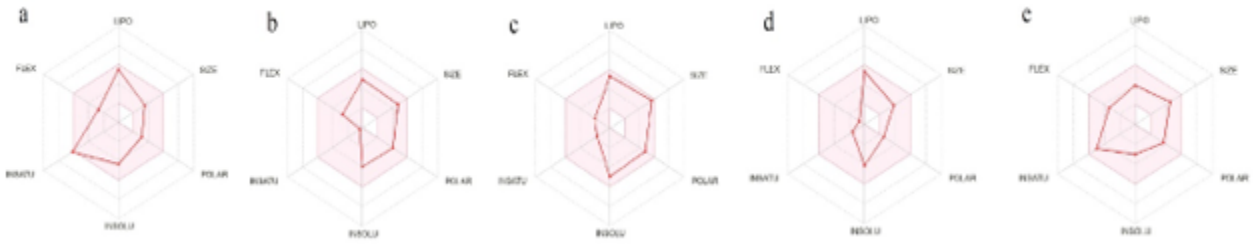

Figure 4

Bioavailability suitable physicochemical space of most active isolates (a) AL17 (b) AL20 (c) AL35 (d) AL38 and (e) AL40

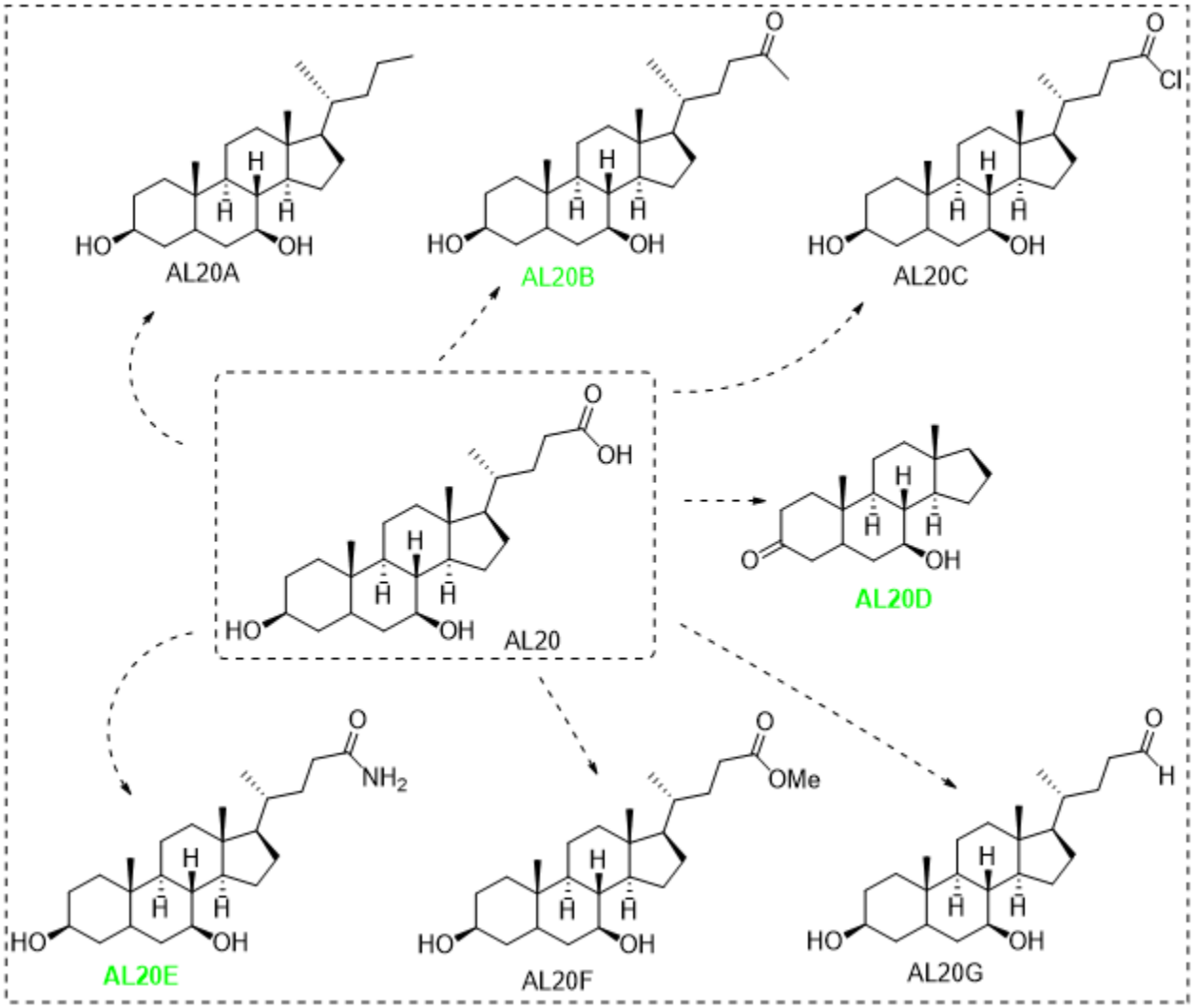

Figure 5

Structure of AL20 isolated from *Jania rubens* and its structurally modified non-toxic derivatives obtained through SAR Study.

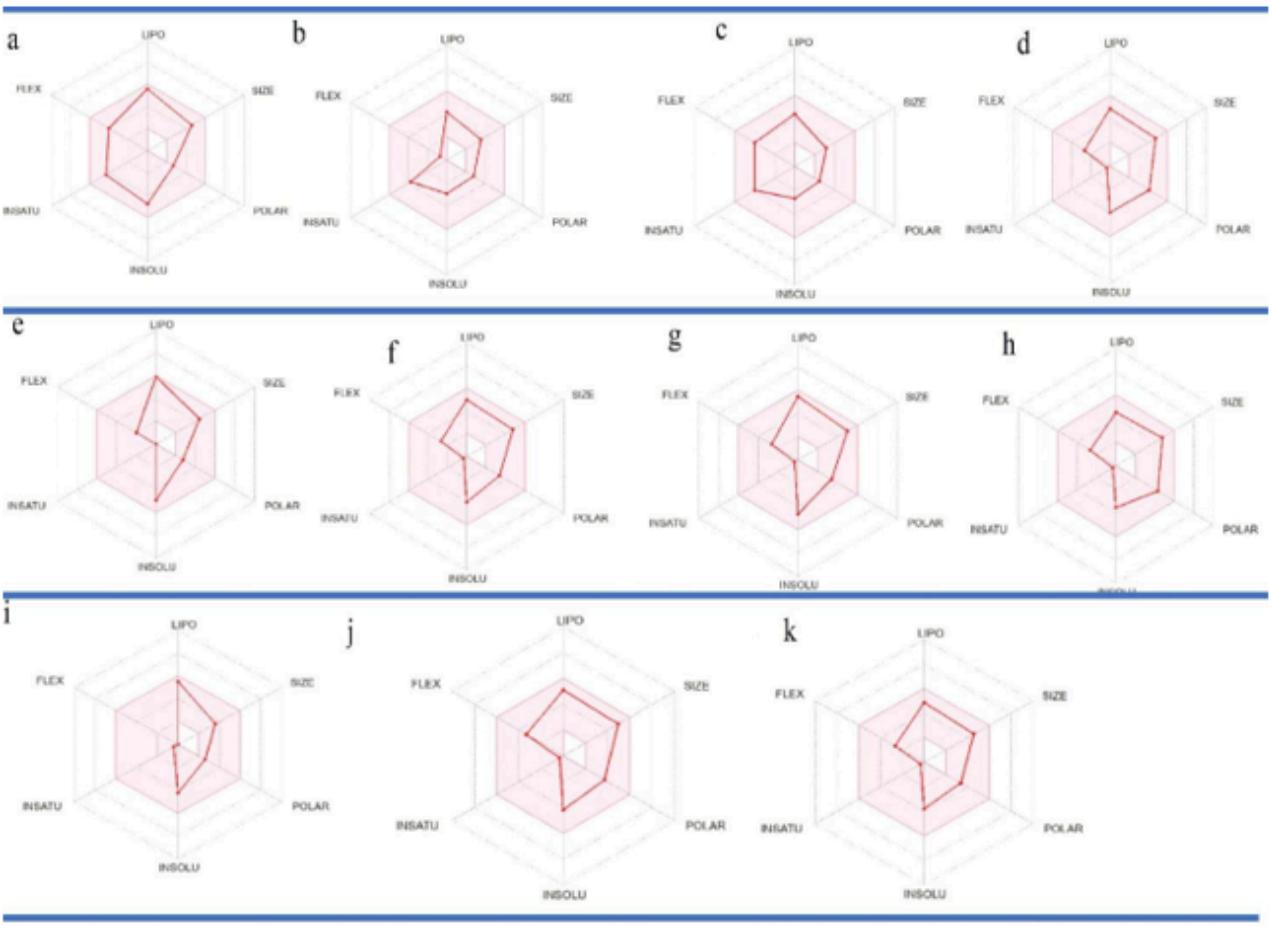

Figure 6

Bioavailability suitable physicochemical space of three Alzheimer's standard drugs and AL20 hypothetical derivatives AL20A-AL20G, (a) donepezil (b) Galantamine (c) Rivastigmine (d) AL20 (e) AL20A (f) AL20B (g) AL20C (h) AL20D (i) AL20E (j) AL20F (k) AL20G

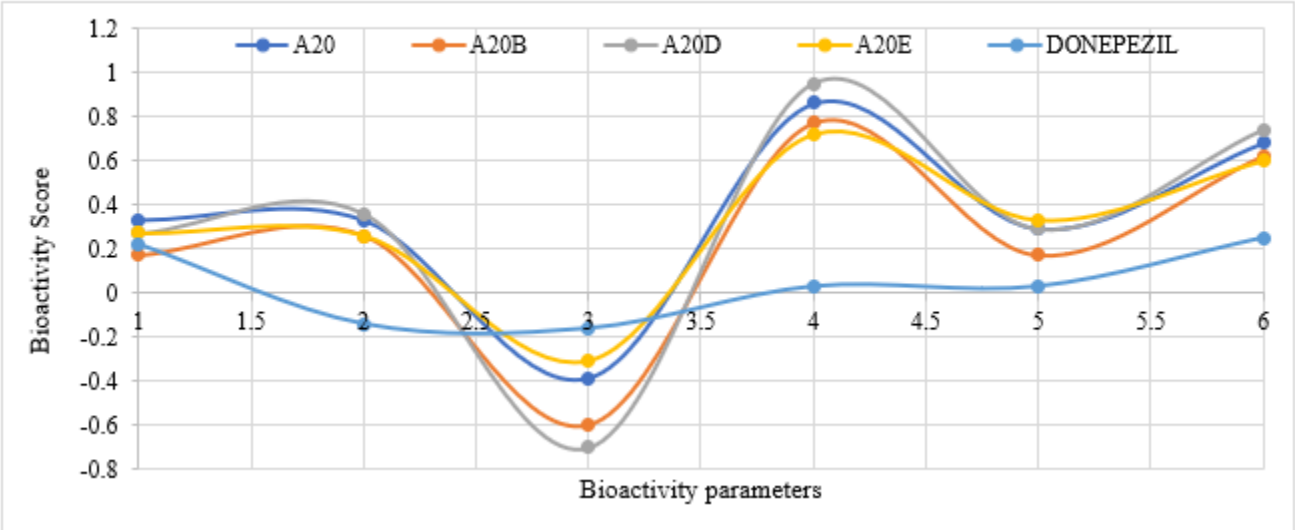

Figure 7

Bioactivity scores of *Jania rubens* phytochemical (AL20), its lead derivatives (AL20B, AL20D and AL20E), and Alzheimer reference drug Donepezil.

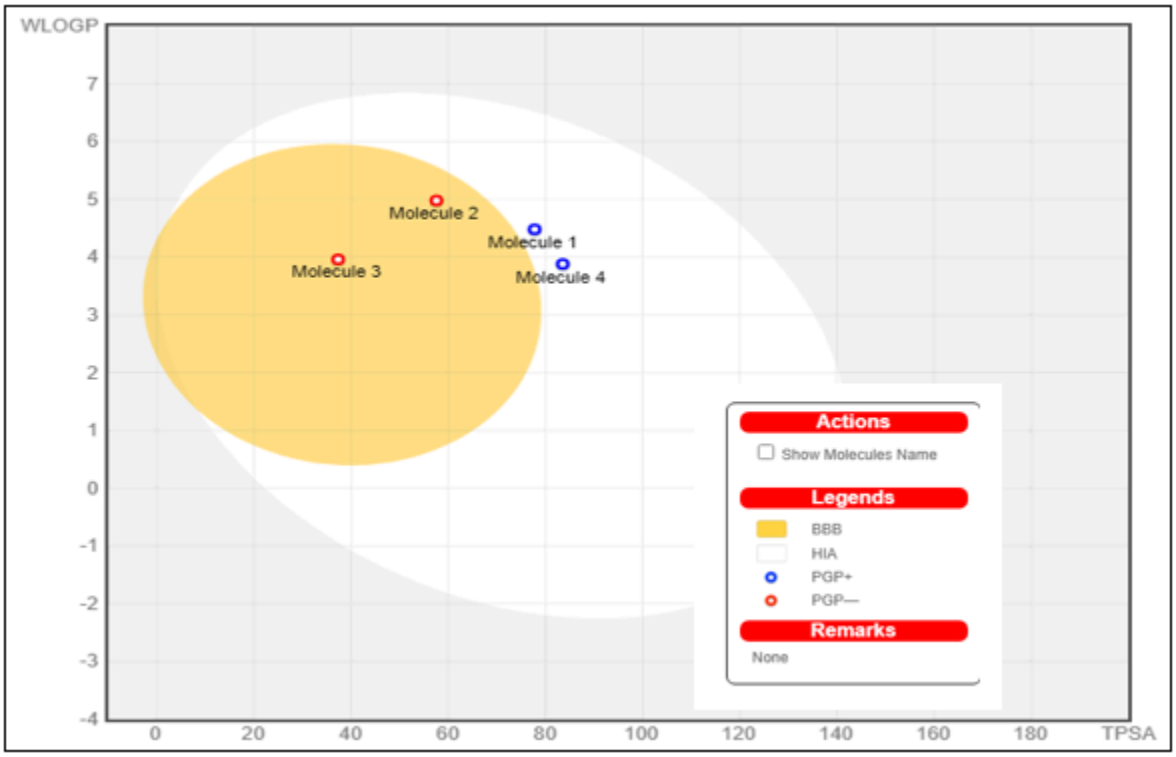

Figure 8

BOILED-Egg model of AL20 and its structurally modified non-toxic derivatives using SwissADME webserver (AL20, AL20B, AL20D, and AL20E represented as Molecules 1, 2, 3 and 4 respectively).

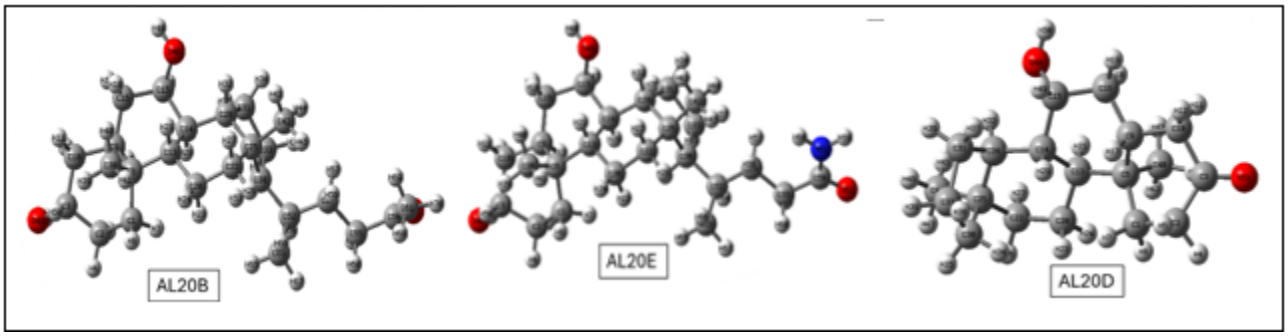

Figure 9

The Geometry Optimization of the Selected AL20s (AL20B, AL20D and AL20E)

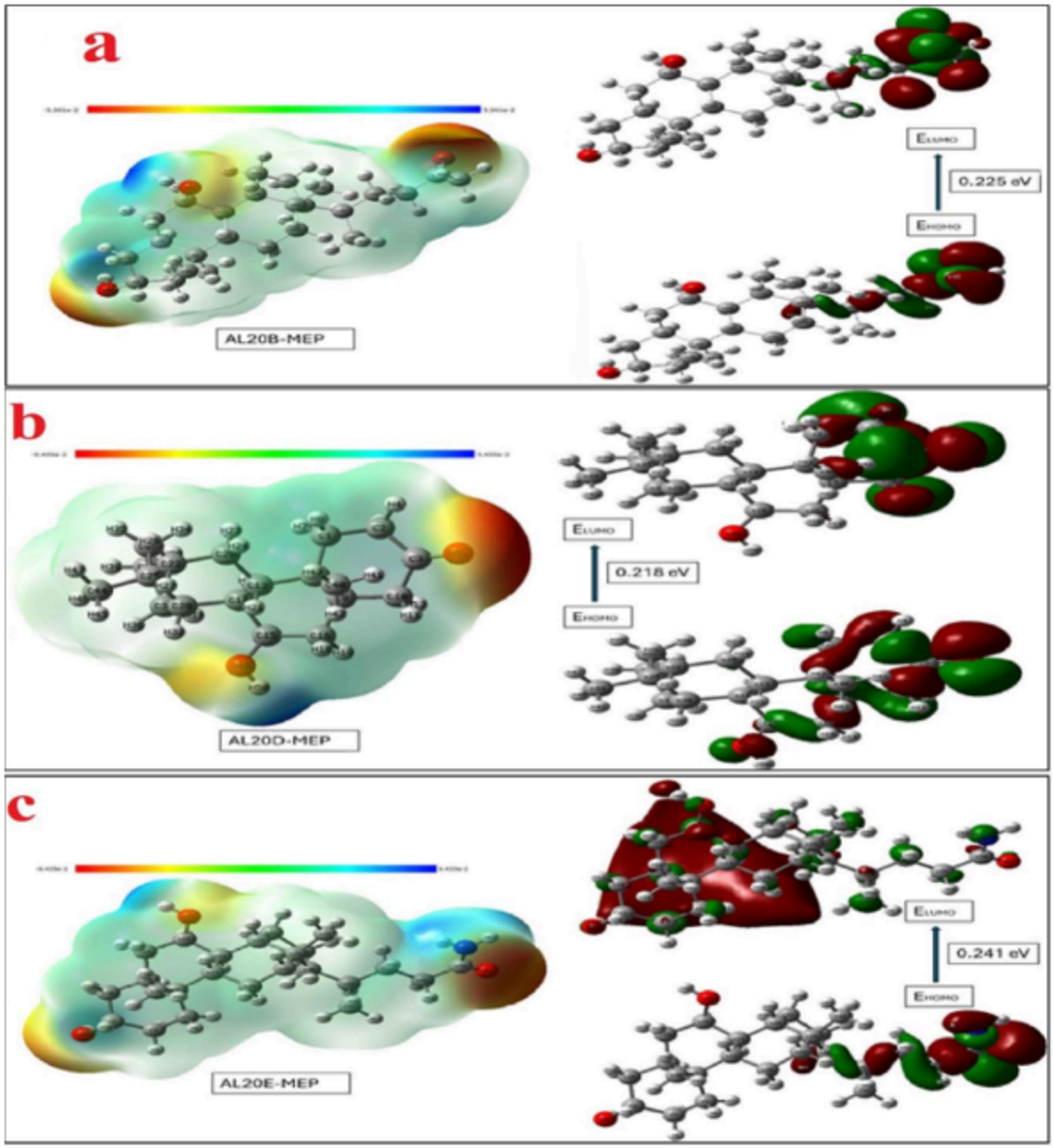

Figure 10

The MEP and HOMO-LUMO transitions of the AL20 series (a) AL20B (b) AL20D and (c) AL20E

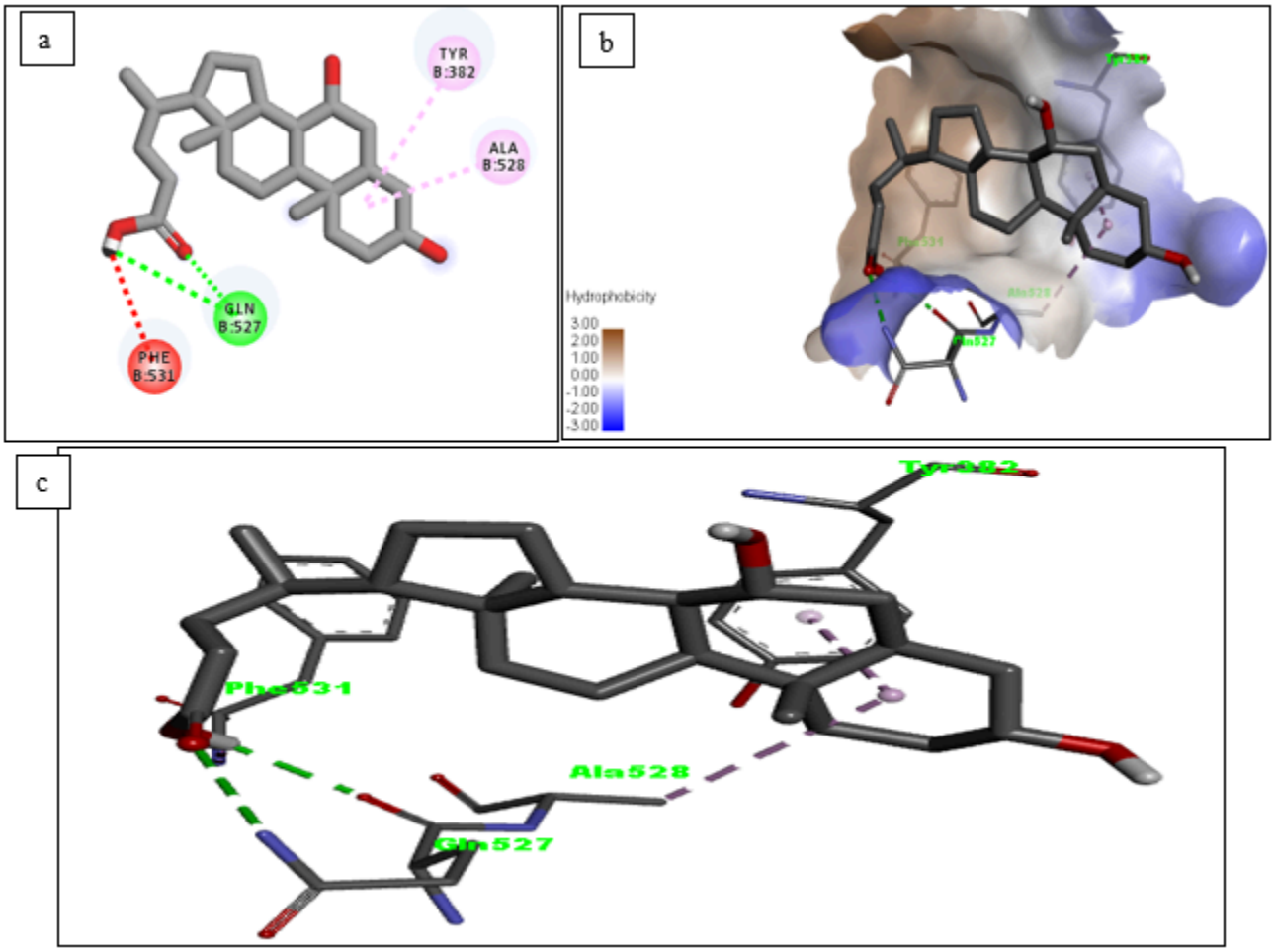

Figure 11

3D structures of 4ey6_**AL20** complex showing (a) bond lengths, (b) hydrophobic interactions and (c) binding residues.

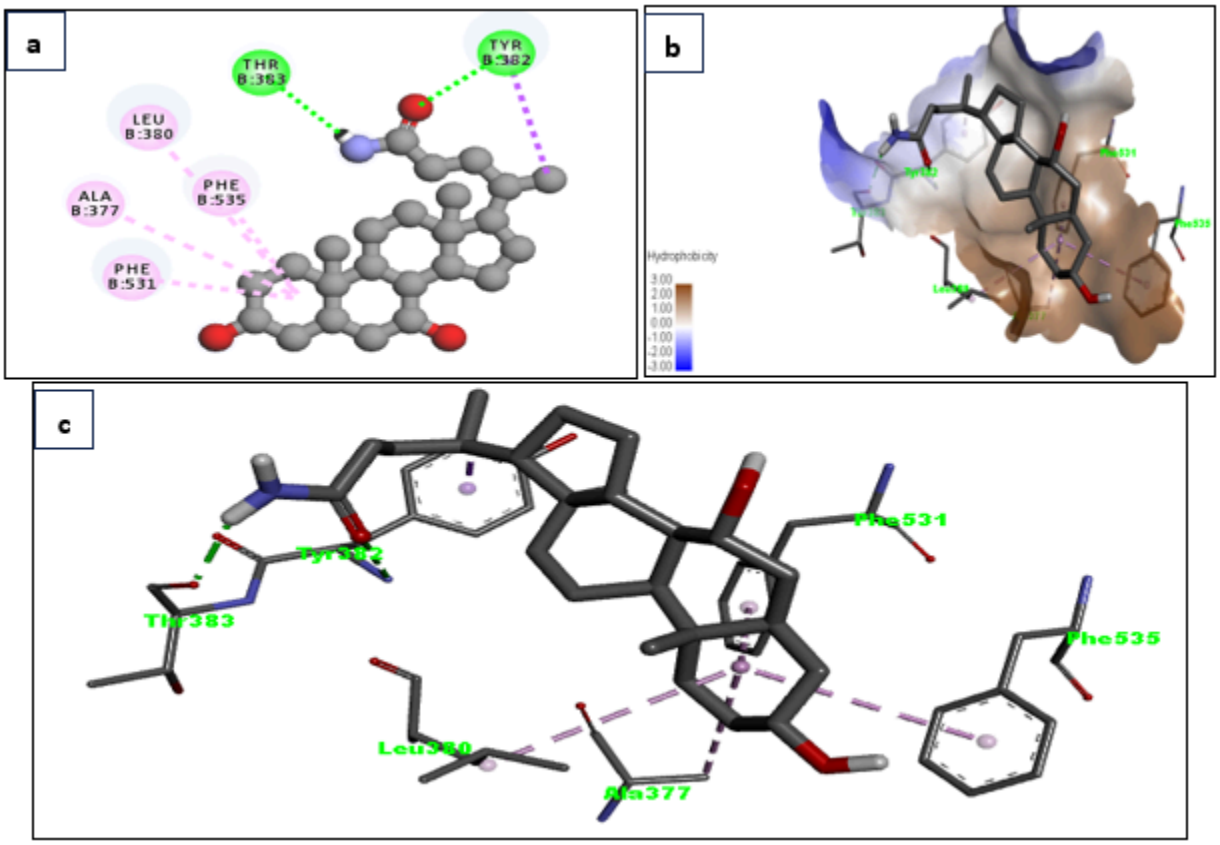

Figure 12

2D and 3D structures of 4ey6_**AL20E** complex showing (a) bond lengths, (b) hydrophobic interactions and (c) binding residues.

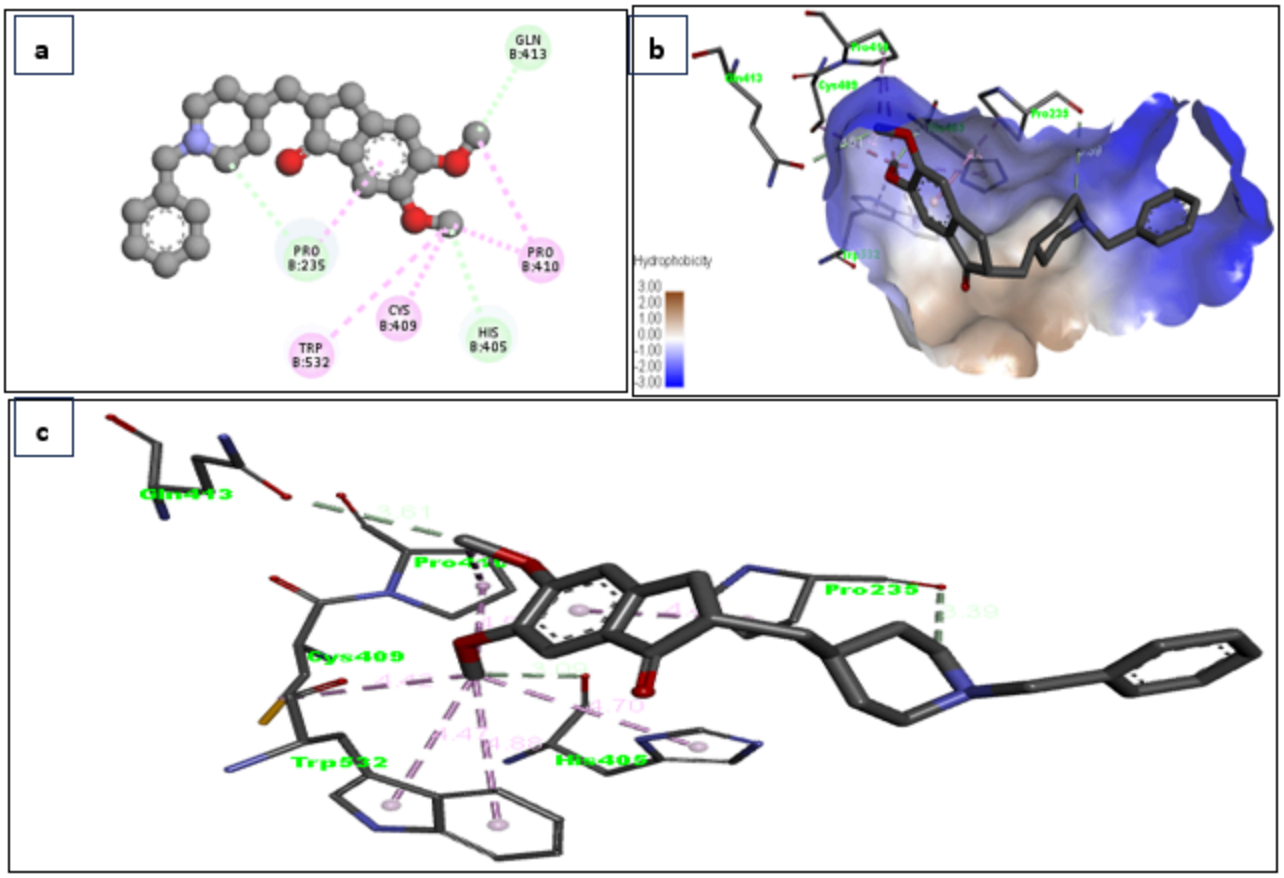

Figure 13

2D and 3D structures of 4ey6_**Donepezil** complex showing (a) bond lengths, (b) hydrophobic interactions and (c) binding residues.

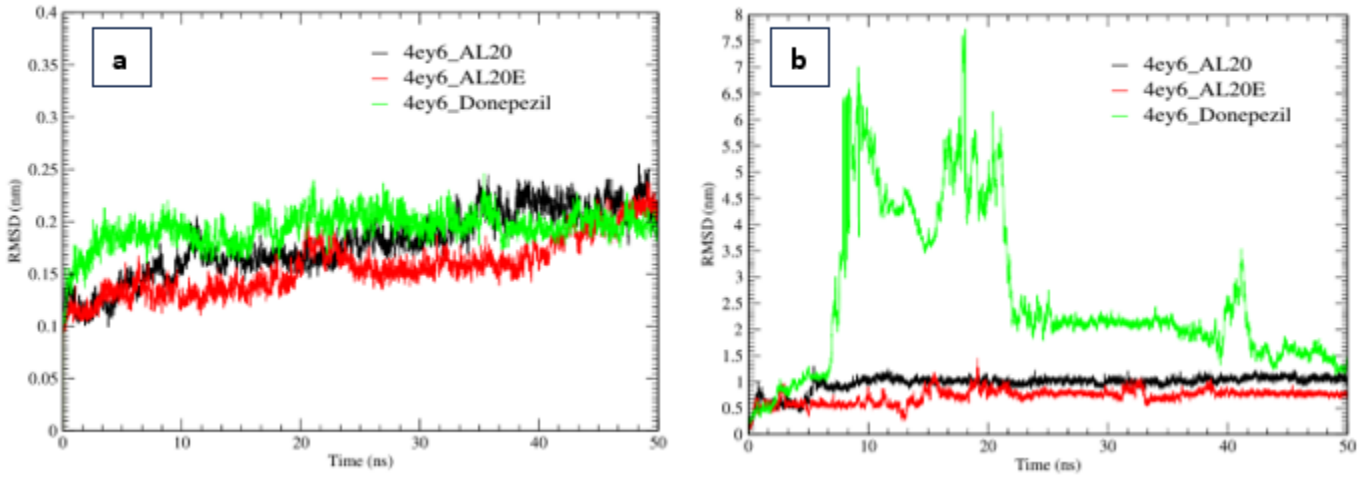

Figure 14

Backbone (a) and ligand (b) root mean square deviation plots for complexes 4ey6_AL20, 4ey6_AL20E and 4ey6_Donepezil

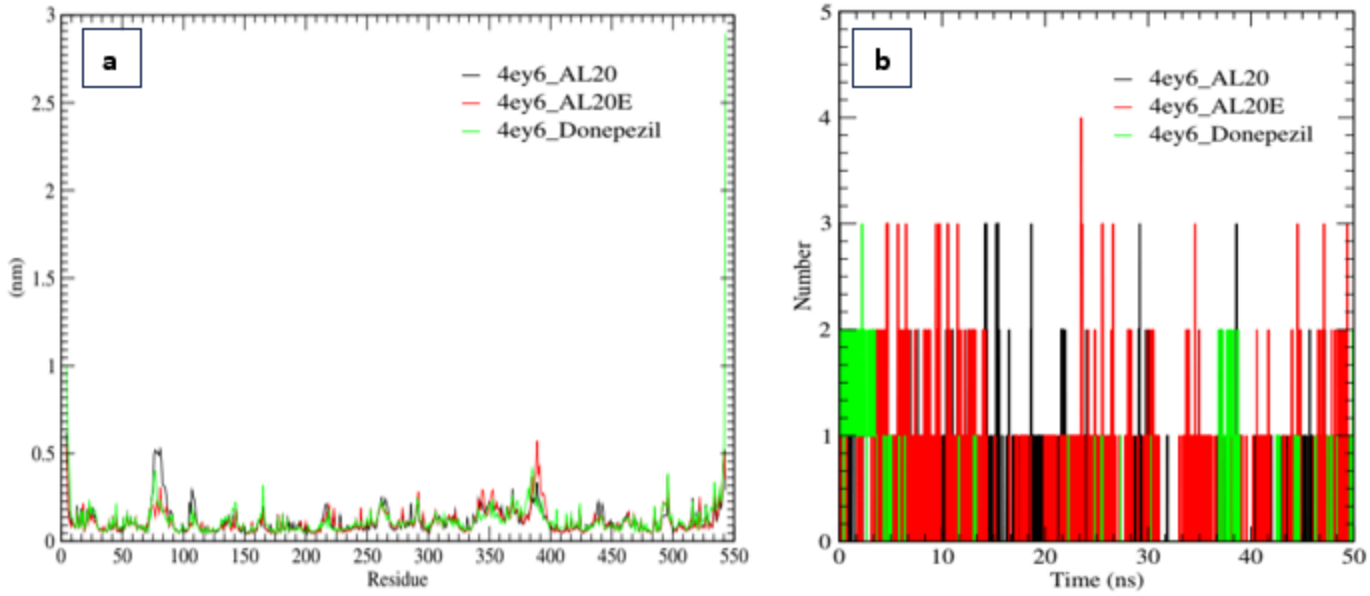

Figure 15

Root mean square fluctuation (a) and hydrogen bonds plots (b) for complexes 4ey6_AL20, 4ey6_AL20E and 4ey6_Donepezil

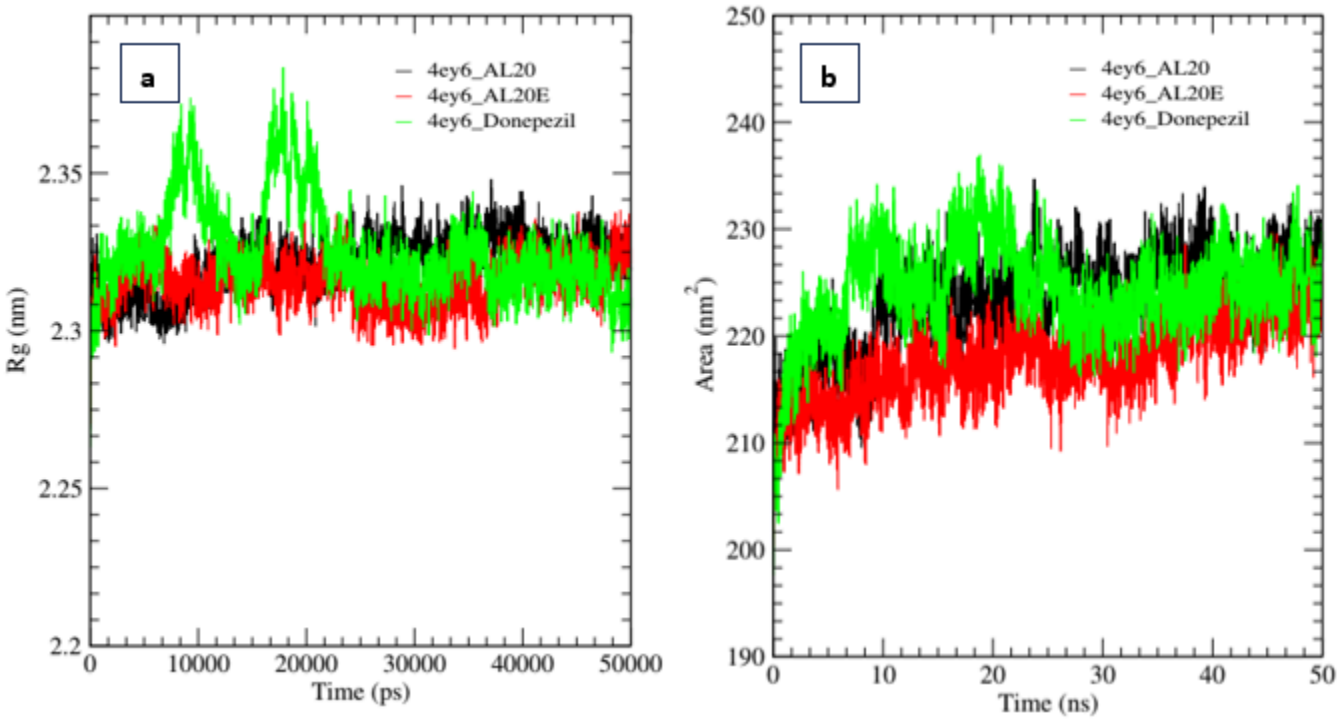

Figure 16

Radius of gyration (a) and Solvent accessibility surface area (SASA) (b) plots for complexes 4ey6_AL20, 4ey6_AL20E and 4ey6_Donepezil

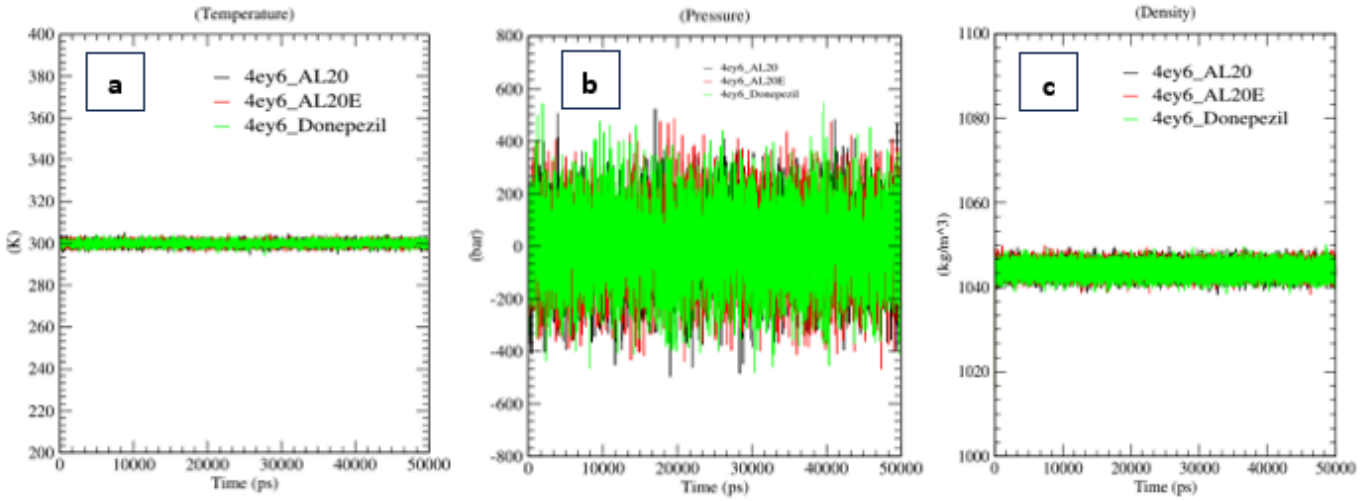

Figure 17

Temperature (a), Pressure (b) and Density (c) energy plots for complexes 4ey6_AL20, 4ey6_AL20E and 4ey6_Donepezil